

# Journal of Biomedical Optics

[SPIEDigitalLibrary.org/jbo](http://SPIEDigitalLibrary.org/jbo)

## ***In vivo* imaging of unstained tissues using a compact and flexible multiphoton microendoscope**

Christopher M. Brown  
David R. Rivera  
Ina Pavlova  
Dimitre G. Ouzounov  
Wendy O. Williams  
Sunish Mohanan  
Watt W. Webb  
Chris Xu

# *In vivo* imaging of unstained tissues using a compact and flexible multiphoton microendoscope

Christopher M. Brown,<sup>a,\*</sup> David R. Rivera,<sup>a,\*</sup>  
Ina Pavlova,<sup>b</sup> Dimitre G. Ouzounov,<sup>a</sup>  
Wendy O. Williams,<sup>c</sup> Sunish Mohanan,<sup>c</sup>  
Watt W. Webb,<sup>a</sup> and Chris Xu<sup>a</sup>

<sup>a</sup>Cornell University, School of Applied and Engineering Physics,  
271 Clark Hall, Ithaca, New York 14853-2501

<sup>b</sup>Rice University, Department of Bioengineering, 6500 Main Street  
Suite 135, Houston, Texas 77030

<sup>c</sup>Cornell University, College of Veterinary Medicine, Ithaca,  
New York 14853-6401

**Abstract.** We use a compact and flexible multiphoton microendoscope (MPME) to acquire *in vivo* images of unstained liver, kidney, and colon from an anesthetized rat. The device delivers femtosecond pulsed 800 nm light from the core of a raster-scanned dual-clad fiber (DCF), which is focused by a miniaturized gradient-index lens assembly into tissue. Intrinsic fluorescence and second-harmonic generation signal from the tissue is epi-collected through the core and inner clad of the same DCF. The MPME has a rigid distal tip of 3 mm in outer diameter and 4 cm in length. The image field-of-view measures 115  $\mu\text{m}$  by 115  $\mu\text{m}$  and was acquired at 4.1 frames/s with 75 mW illumination power at the sample. Organs were imaged after anesthetizing Sprague-Dawley rats with isoflurane gas, accessing tissues via a ventral-midline abdominal incision, and isolating the organs with tongue depressors. *In vivo* multiphoton images acquired from liver, kidney, and colon using this device show features similar to that of conventional histology slides, without motion artifact, in ~75% of imaged frames. To the best of our knowledge, this is the first demonstration of multiphoton imaging of unstained tissue from a live subject using a compact and flexible MPME device. © 2012 Society of Photo-Optical Instrumentation Engineers (SPIE). [DOI: 10.1117/1.JBO.17.4.040505]

Keywords: endoscopy; fiber optic applications; imaging; medical imaging; microscopy; multiphoton processes.

Paper 12043L received Jan. 20, 2012; revised manuscript received Feb. 28, 2012; accepted for publication Mar. 1, 2012; published online Apr. 9, 2012.

## 1 Introduction

Minimally invasive *in vivo* diagnostic imaging has the potential to minimize patient discomfort by providing a diagnosis without tissue removal, speed diagnosis, reduce cost by allowing for real-time determination of tissue disease state, and generate a diagnostic yield equivalent to conventional histopathology. Among minimally invasive diagnostic techniques, multiphoton microscopy is promising because it is capable of acquiring label-free tissue

images at high resolution that provide diagnostic information similar to that obtained from tissue biopsies processed into histology slides.<sup>1-3</sup> For multiphoton microscopy to successfully translate from research to clinical settings, a compact and flexible multiphoton microendoscope (MPME) must be developed that combines small size to access a wide variety of organs *in vivo*, high frame rate to mitigate motion artifact, and high-quality imaging capability to produce images that are useful for disease diagnosis (i.e., capable of subcellular resolution allowing for image acquisition of cellular details such as nucleus size and nucleus/cytoplasm ratio). Previously, researchers have acquired unstained images *in vivo* using GRIN lenses in combination with table-top two-photon laser scanning microscopes.<sup>4,5</sup> In this paper, we demonstrate *in vivo* imaging of unstained tissues using a compact and flexible MPME. The fiber delivery and the small size (3 mm OD and 4 cm rigid length) of the MPME will allow it to be used in a similar fashion to a number of clinical endoscopic devices.

Though there have been significant efforts to develop compact and flexible endoscopic devices based upon microelectromechanical systems<sup>6-8</sup> and devices that operate nonresonantly,<sup>9-12</sup> to date, the devices that have the best combination of small size, high frame rate, and high-quality image acquisition are distally resonant-scanned optical-fiber systems.<sup>13-19</sup> In these devices, illumination light is delivered through an optical fiber into an objective lens that focuses and epi-collects light from tissue. In distally scanned systems, the optical fiber is mounted to one or more actuators that deflect the fiber tip in a two-dimensional resonant spiral scan,<sup>13-16</sup> resonant Lissajous scan,<sup>18,19</sup> or a combined resonant-nonresonant raster scan pattern.<sup>17</sup> As described previously, an advantage of the resonant-nonresonant raster scanner compared with the resonant spiral or Lissajous scanner is increased uniformity of pixel-dwell-time, and thus increased uniformity of illumination and light collection across the image field-of-view (FOV).<sup>17</sup>

Research groups that have developed these miniature *in vivo* imaging devices use them for either neural research<sup>6,13,18</sup> or for clinical microendoscopy.<sup>10,11</sup> Groups that have developed devices for *in vivo* imaging of the brain function have sought to conduct multiphoton imaging of rat cortical blood flow and neural activity using fluorescently labeled dextran and Ca indicator dyes. Groups that have developed devices for *in vivo* clinical imaging have sought to conduct multiphoton imaging of kidney tissue stained using Fluorescein<sup>11</sup> and to conduct narrow-band imaging of various fluorescently labeled organs throughout the GI tract.<sup>10</sup> Although, dyes and stains that improve the contrast of imaged tissue are acceptable for research purposes, it is highly desirable that clinical imaging of human tissue be independent of exogenous contrast agents for acquisition of quality images. To date, few contrast agents have been clinically approved for use in human patients (e.g., Fluorescein, Indocyanine Green, and Acriflavine in certain parts of the world) due to dye toxicity. Multiphoton microscopy has demonstrated the capability to image intrinsic fluorescence and second-harmonic generation (SHG) signal in tissue without requiring exogenous stains or dyes. Here, we describe the use of an MPME device to acquire *in vivo* images from unstained kidney, liver, and colon of an anesthetized rat. To the best of our knowledge, this is the first demonstration of *in vivo* multiphoton image acquisition from unstained tissue using a compact and flexible MPME device.

\*These authors contributed equally.

Address all correspondence to: Christopher M. Brown, Cornell University, School of Applied and Engineering Physics, 271 Clark Hall, Ithaca, New York 14853-2501; Tel: (607)255-8034; E-mail: [cmb378@cornell.edu](mailto:cmb378@cornell.edu)

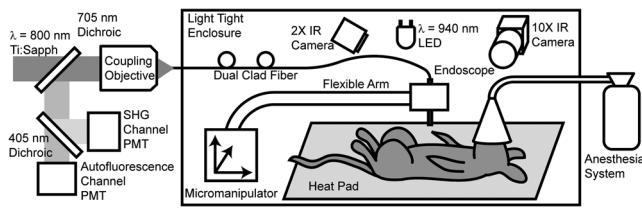


**Fig. 1** *In vivo* imaging experimental layout. Note that the 800 nm excitation light is precompensated for the DCF dispersion prior to fiber coupling.

The MPME uses a femtosecond source (Mai Tai HP, Spectra Physics) to deliver 800 nm light through the core of a raster-scanned dual-clad optical fiber (DCF SM-9/105/125-20A, Nufern). The focusing lens is a Gradient Refractive Index (GRIN) objective (GT-MO-080-018-810, GRINTECH). Intrinsic fluorescence and SHG signal are epi-collected through the core and inner clad of the dual-clad fiber, proximally split into two collection channels using a dichroic beam splitter (Di01-R405-25 × 36, Semrock), and detected using two PMTs (R7600U-200, Hamamatsu) as shown in Fig. 1. The MPME acquires images at 4.1 frames/s with a FOV<sub>XY</sub> of 115 × 115 μm. Lateral and axial two-photon resolutions measured 0.8 and 10 μm (full width at half maximum), respectively, in the image plane. For *in vivo* imaging, illumination power at the sample is approximately 75 mW, below the threshold for mutagenicity.<sup>20</sup> Additional details regarding the MPME, dispersion compensation system, and pulse characterization of the illumination light are described in previous publications.<sup>17,21</sup>

In this experiment, the imaging apparatus was housed inside a light-tight enclosure to reduce background signal detected by the device (Fig. 1). Inside the enclosure, MPME position was controlled remotely by mounting the device on a flexible arm (FLEX-BAR Positioning Arm, Flexbar Machine Corp.) allowing for six degrees of freedom of gross movement. The flexible arm was mounted on a precision motorized micromanipulator (MP-285, Sutter Instrument Co.) allowing for submicron XYZ axis motion control of the endoscope. An infrared (IR) imaging system was used to assist with navigation of the endoscope and monitor the respiration rate of the anesthetized rat to ensure normal breathing during the imaging procedure. The imaging system used two IR (illumination wavelength 940 nm) LEDs (M940L2, Thorlabs) to illuminate the animal while acquiring images from two CCD camera systems. Illumination light from the IR LEDs was blocked from the MPME PMTs using a short-pass filter (FF01-720/SP-25, Semrock). The IR filter, combined with the poor quantum efficiency of the PMTs at the IR illumination wavelength, allowed for simultaneous MPME and IR wide-field imaging during the experimental procedure. Together, the two IR imaging systems allowed for 10× and 2× magnification IR imaging of the device and anesthetized rat (Fig. 2).

A male rat (250 to 350 grams, Sprague-Dawley, Charles River Laboratories International, Inc.) model was used in this experiment. Prior to surgery, the rat was sedated in an induction chamber with a gas anesthetic (~5% isoflurane-oxygen mixture). After reaching the appropriate level of sedation for surgery, the animal was fitted with a nose cone to maintain the sedation (~2 to 3% isoflurane-oxygen mixture), placed on a temperature-controlled heat pad (set to 36°C) to maintain body temperature and mechanically restrained in a dorsal recumbent position. A small ventral-midline abdominal incision was made to expose the internal organs to the MPME. After imaging the kidney and the liver, a second incision was made in the colon to expose its inner surface

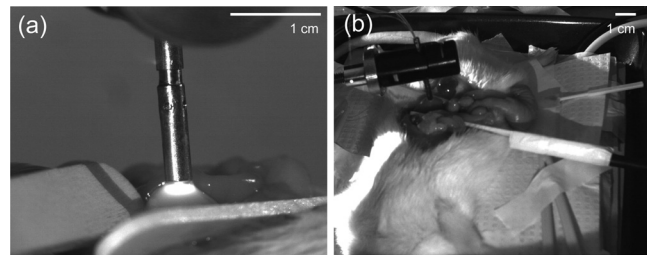


**Fig. 2** Infrared camera images: (a) 10× view of 3 mm OD endoscope acquiring *in vivo* kidney image; (b) 2× view of rat and mounted endoscope.

to the device. Prior to imaging each organ, the organ was isolated then elevated with tongue depressors to reduce motion artifact (Fig. 2). The endoscope was then maneuvered into position for image acquisition using the flexible arm and micromanipulator. A total of 10 rats were imaged using these procedures. After the initial iterations, we achieved a consistent procedural throughput for the last several runs where the entire imaging session (e.g., imaging kidney, liver, and colon) required approximately 40 min. All animal procedures were conducted in accordance with a Cornell University Institutional Animal Care and Use Committee approved protocol and relevant standard operating procedures.

During the *in vivo* imaging sessions, the image plane of the MPME was positioned ~20 to 30 μm below the tissue surface to obtain the *en face* unstained, unaveraged *in vivo* MPME images shown in Figs. 3 and 4. Due to axial motion of the live tissue relative to the MPME image plane, images acquired may be above or below this depth. The recognizable tissue features were highly consistent in all imaged rats. These images show many features that are recognizable in histological tissue samples.<sup>22</sup> Figure 3(a) shows an image of intrinsic fluorescent signal in the rat kidney. In this image, optical cross-sections of tubular nephrons are visible in the periphery of the organ along with features such as cells, renal tubules, renal interstitium, and renal lumen. Figure 3(b) shows an image of intrinsic fluorescent signal from the interior wall of the rat colon. This image shows an optical cross-section of a colon crypt. Figure 4(a), 4(b), and Video 1 show intrinsic fluorescence (pseudocolored green) and SHG (gray) images ~20 to 30 μm below the surface of the rat liver. These images show hepatocytes (i.e., functional liver cells)

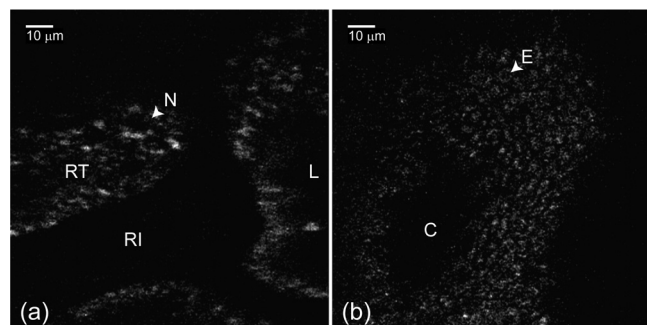


**Fig. 3** Unaveraged, unstained multiphoton endoscope images of rat kidney and colon. Images show intrinsic fluorescence emission (420–690 nm): (a) Image of superficial kidney renal cortex, approximately 20 μm below the surface of the organ showing epithelial cellular nuclei (N) 5 to 10 μm in diameter, renal tubules (RT) composed of epithelial cells, renal interstitium (RI)—the loose connective tissue and vascular supply in the kidney, and renal lumen (L) inside the renal tubules; (b) image 20 to 30 μm below the surface of the interior colon showing a cross-sectional view of a crypt (C) and a variety of enterocyte cells lining the intestine (E). Note that dark cellular nuclei are viewable in many of these cells.

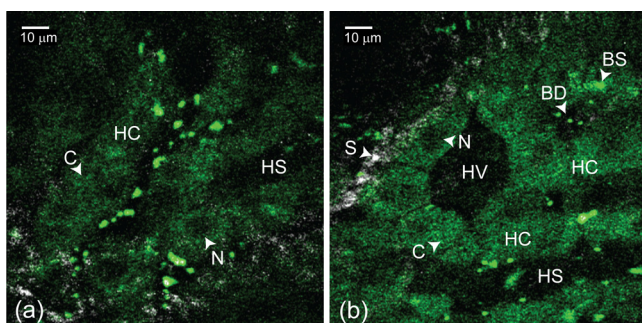


**Fig. 4** Unaveraged, unstained multiphoton endoscope images of rat liver located approximately 20  $\mu\text{m}$  below organ surface. The pseudo-color images show grey SHG signal ( $<405\text{ nm}$ ) and green intrinsic fluorescent emission (420 to 690 nm). (a) Liver image shows 20 to 30  $\mu\text{m}$  diameter hepatocytes with a dark 5–10  $\mu\text{m}$  diameter nucleus (N) and bright surrounding cytoplasm (C), hepatic chords (HC) composed of chains of hepatocytes, and a hepatic sinusoid (HS)—the blood filled space between hepatic chords. (b) Liver image (also shown in [Video 1](#)) shows features including: bile ductile (BD), bile salts (BS), septa (S)—a fine fibrillar connective tissue that covers the surface of the hepatocytes, and a hepatic venule (HV). ([Video 1](#), QuickTime, MOV, 3.8 MB). [URL: <http://dx.doi.org/10.1117/1.JBO.17.4.040505.1>]

surrounded by a collagenous tissue capsule. The hepatocytes are arranged in cords, forming structural units. The blood-filled spaces between the cords are sinusoids. Since blood is a strong light absorber, we see an absence of intrinsic signal in the sinusoid. Strong SHG signal can be seen in the septa of the liver. Images in [Figs. 3 and 4](#) were interpreted with the assistance of a certified pathologist. When imaging kidney, liver, and colon tissue with this device, over  $\sim 75\%$  of recorded images were free of streaking or warping of features within the image frame even though the organ moves relative to the MPME due to respiration and heart beat, as shown in [Video 1](#). This can be credited to rigid mounting of the endoscope during image acquisition, isolating tissue while imaging, the 4.1 frame/s image acquisition speed, and the high uniformity of the resonant-nonresonant fiber scanner. The demonstrated device can be further improved by achieving faster frame rates with high signal-to-noise ratio, distal axial sectioning, larger image FOVs while maintaining high-image resolution, and decreasing the device size. Several recent developments are designed to address these issues. For example, by incorporating lensed fibers a larger FOV can be achieved in a miniature endoscope.<sup>23</sup> Furthermore, a higher frame rate and axial sectioning can be achieved by incorporating a multifocal approach in the MPME.<sup>24</sup> To the best of our knowledge, this research demonstrates the first multiphoton images from unstained tissue in a live animal using a compact and flexible MPME device. These images show many of the features that are commonly seen in biopsied histopathology slides from these tissues, indicating the potential of the MPME device for *in vivo* diagnostics of tissue health.

#### Acknowledgments

The authors thank Dr. Manu Jain for assistance with interpretation of *in vivo* images. Our project was supported by NIH/NIBIB Grant R01-EB006736 “Development of Medical Multiphoton Microscopic Endoscopy” and the NIH/NCI Grant R01-CA133148.

#### References

1. S. Mukherjee et al., “Human bladder cancer diagnosis using multiphoton microscopy,” *Proc. SPIE* **7161**, 716117 (2009).
2. I. Pavlova et al., “Multiphoton microscopy and microspectroscopy for diagnostics of inflammatory and neoplastic lung,” *J. Biomed. Opt.* **17**(3), 036014 (2012).
3. M. C. Skala et al., “Multiphoton microscopy of endogenous fluorescence differentiates normal, precancerous, and cancerous squamous epithelial tissues,” *Cancer Res.* **65**(4), 1180–1186 (2005).
4. K. Konig et al., “Clinical two-photon microendoscopy,” *Microsc. Res. Tech.* **70**(5), 398–402 (2007).
5. M. E. Llewellyn et al., “Minimally invasive high-speed imaging of sarcomere contractile dynamics in mice and humans,” *Nature* **454**(7205), 784–788 (2008).
6. W. Piyawattanametha et al., “*In vivo* brain imaging using a portable 2.9 g two-photon microscope based on a microelectromechanical systems scanning mirror,” *Opt. Lett.* **34**(15), 2309–2311 (2009).
7. L. Fu et al., “Three-dimensional nonlinear optical endoscopy,” *J. Biomed. Opt.* **12**(4), 040501 (2007).
8. S. Tang et al., “Design and implementation of fiber-based multiphoton endoscopy with microelectromechanical systems scanning,” *J. Biomed. Opt.* **14**(3), 034005 (2009).
9. B. H. Hendriks et al., “High-resolution resonant and nonresonant fiber-scanning confocal microscope,” *J. Biomed. Opt.* **16**(2), 026007.
10. M. Goetz et al., “*In vivo* confocal real-time mini-microscopy in animal models of human inflammatory and neoplastic diseases,” *Endoscopy* **39**(4), 350–356 (2007).
11. H. Bao et al., “Fast handheld two-photon fluorescence microendoscope with a 475 microm  $\times$  475 microm field of view for *in vivo* imaging,” *Opt. Lett.* **33**(12), 1333–1335 (2008).
12. J. Sawinski and W. Denk, “Miniature random-access fiber scanner for *in vivo* multiphoton imaging,” *J. Appl. Phys.* **102**(3), 034701 (2007).
13. C. J. Engelbrecht et al., “Ultra-compact fiber-optic two-photon microscope for functional fluorescence imaging *in vivo*,” *Opt. Express* **16**(8), 5556–5564 (2008).
14. M. T. Myaing, D. J. MacDonald, and X. Li, “Fiber-optic scanning two-photon fluorescence endoscope,” *Opt. Lett.* **31**(8), 1076–1078 (2006).
15. E. J. Seibel and Q. Y. Smithwick, “Unique features of optical scanning, single fiber endoscopy,” *Lasers Surg. Med.* **30**(3), 177–183 (2002).
16. Y. Zhao, H. Nakamura, and R. J. Gordon, “Development of a versatile two-photon endoscope for biological imaging,” *Biomed. Opt. Express* **1**(4), 1159–1172 (2011).
17. D. R. Rivera et al., “Compact and flexible raster scanning multiphoton endoscope capable of imaging unstained tissue,” *Proc. Natl. Acad. Sci. U. S. A.* **108**(43), 17598–17603 (2011).
18. F. Helmchen et al., “A miniature head-mounted two-photon microscope. high-resolution brain imaging in freely moving animals,” *Neuron* **31**(6), 903–912 (2001).
19. T. Wu et al., “Two-dimensional scanning realized by an asymmetry fiber cantilever driven by single piezo bender actuator for optical coherence tomography,” *Opt. Express* **17**(16), 13819–13829 (2009).
20. J. M. Dela Cruz et al., “Feasibility of using multiphoton excited tissue autofluorescence for *in vivo* human histopathology,” *Biomed. Opt. Express* **1**(5), 1320–1330.
21. M. E. Durst, D. Kobat, and C. Xu, “Tunable dispersion compensation by a rotating cylindrical lens,” *Opt. Lett.* **34**(8), 1195–1197 (2009).
22. L. P. Gartner and J. L. Hiatt, *Color Textbook of Histology* W. B. Saunders, Philadelphia (2001).
23. D. R. Rivera et al., “Use of a lensed fiber for a large-field-of-view, high-resolution, fiber-scanning microendoscope,” *Opt. Lett.* **37**(5), 881–883 (2012).
24. D. R. Rivera et al., “Multifocal multiphoton endoscope,” *Opt. Lett.* **37**(8), 1349–1351 (2012).